Peer-reviewed version available at *Cancers* **2020**, *12*, 1331; doi:10.3390/cancers12051331

Article

Gold Nanoparticle Mediated Multi-Modal CT Imaging of Hsp70 Membrane Positive Tumors

Melanie A. Kimm[1], Maxim Shevtsov[2,3,4], Caroline Werner[2], Wolfgang Sievert[2], Wu Zhiyuan[2], Oliver Schoppe[2,5], Bjoern H. Menze[2,5], Ernst J. Rummeny[1], Roland Proksa[6], Olga Bystrova[4], Marina Martynova[4], Gabriele Multhoff[2,§,*] and Stefan Stangl[2,§,*]

[1]Department of Diagnostic and Interventional Radiology, Klinikum rechts der Isar der Technischen Universität München, Munich, Germany; Melanie.Kimm@tum.de; Ernst.Rummeny@tum.de;

[2]Central Institute for Translational Cancer Research (TranslaTUM), Klinikum rechts der Isar der Technischen Universität München, Munich, Germany; Maxim.Shevtsov@tum.de; C.Werner@tum.de; Wolfgang.Sievert@tum.de; Gabriele.Multhoff@tum.de; Stefan.Stangl@tum.de

[3]Pavlov First Saint Petersburg State Medical University, St. Petersburg, Russia

[4]Institute of Cytology of the Russian Academy of Sciences (RAS), Russia, St. Petersburg

[5]Institute for Advanced Studies, Department of Informatics, Technical University of Munich, Munich, Germany: Oliver.Schoppe@tum.de; Bjoern.Menze@tum.de;

[6]Philips GmbH Innovative Technologies, Research Laboratories Hamburg, Germany, roland.proksa@philips.com

*Correspondence: Dr. rer. nat. Stefan Stangl and Prof. Dr. rer. nat. Gabriele Multhoff

Dr. rer. nat. Stefan Stangl

TranslaTUM, Klinikum rechts der Isar

Technische Universität München

Einsteinstr. 25

D-81675 Munich

Germany

Stefan.Stangl@tum.de

Phone: +49 89 4140-6013

Fax: +49 89 4140-4299

&

Prof. Dr. rer. nat. Gabriele Multhoff

TranslaTUM, Klinikum rechts der Isar

Technische Universität München

Einsteinstr. 25

D-81675 Munich

Germany

Gabriele.Multhoff@tum.de

Phone: +49 89 4140-4514

Fax: +49 89 4140-4299

Received: date; Accepted: date; Published: date

Abstract: Imaging techniques such as computed tomographies (CT) play a major role in clinical imaging and diagnosis of malignant lesions. In recent years, spectral CT has emerged in the field of computed tomographies, utilizing detailed information from extracted spectral parameters of the specimen. Metal nanoparticle platforms enable effective payload delivery for this technique. Due to the possibility of surface modification, metal nanoparticles are predestined to facilitate molecular tumor targeting.

In this work, we demonstrate the feasibility of anti-plasma membrane Heat shock protein 70 functionalized gold nanoparticles (AuNPs) for tumor specific multimodal imaging. Membrane-associated Hsp70 is exclusively presented on the plasma membrane of malignant cells of multiple tumor entities, but not on corresponding normal tissue cells, predestining this target epitope for tumor-selective *in vivo* targeting.

In vitro microscopical analysis revealed the presence of cmHsp70.1-AuNP in the cytosol of tumor cell lines, being internalized via the endosomal-lysosomal pathway. In tumor bearing mice the biodistribution as well as the intratumorally enrichment of AuNP were examined 24h after i.v. application, *in vivo*. In parallel to spectral CT analysis, histological analysis confirmed the presence of tumor cells. In contrast to control NP, a significant enrichment of cmHsp70.1-AuNPs has been detected selectively in tumors of different preclinical mouse models. Furthermore, the biodistribution of AuNP, following i.v. injection, was analyzed by a machine-learning approach on digitalized slides.

In summary, utilizing mHsp70 on tumor cells for guidance of cmHsp70.1 antibody functionalized nanoparticles enables sufficient enrichment and uniform distribution of AuNPs in mHsp70-expressing tumor cells, adequate for various microscopical imaging techniques and spectral-CT-based tumor delineation, *in vivo*.

Keywords: gold nanoparticle, heat shock protein 70, molecular imaging, biomarker, spectral-CT, k-edge imaging

1. Introduction

Detection of all malignant tumor cells in a patients´ body is a prerequisite for a successful treatment. In established clinical routine, combined positron emission tomography (PET)/computed tomography (CT) imaging is commonly used for

tumors exceeding 0.5–1 cm^3. For standard clinical PET imaging, ^{18}F-Glucose is often used as a PET tracer. However, glucose-based PET/CT imaging faces disadvantages, such as false-positive and/or false-negative signals, e.g. triggered by the fact that only metabolically active, but not resting cells can be visualized, the low tumor-to-background contrast and the relatively low resolution of this technique [1]. With improved settings, a spatial resolution of 2 mm is technically feasible, as demonstrated in patients with prostate cancer [2].

The introduction of gold nanoparticle-based contrast agents added a new value to imaging techniques. Functionalization of novel metal-based nanoparticles with tumor-specific antibodies [3] and their utilization in imaging techniques such as photoacoustic signal transduction or CT combine the advantages of molecular, tumor specific imaging with the unique attributes of Au-NPs in clinical imaging, particularly in spectral-CT. This technology allows spectral imaging as it employs a photon-counting detector which registers the interactions of individual photons which enables to create an energy spectrum which can subsequently be converted into a color image. In addition, a non-spectral attenuation image can be acquired at the same time. This allows for precise spatial information of the spectral image with high resolution. Notably, signals delivered by gold can be

Peer-reviewed version available at Cancers 2020, 12, 1331; doi:10.3390/cancers12051331

efficiently isolated. With the emergence of clinical SPECT scanners, the need of tumor-specific contrast agents has further increased.

For *in vivo* application, it is essential that the applied nanoparticles are nontoxic, biodegradable or inert and transportable in the blood and lymph system. Biocompatible camouflage of the NP surface is a prerequisite to avoid immediate and quantitative uptake by macrophages. Small nanosized gold particles (< 100nm) demonstrated to be beneficial for utilization in clinical applications [4-6]. Apart from the formulation of the NPs, tumor imaging with nanoparticle-based contrast agents can be further improved and specified by functionalization with antibodies targeting tumor-specific, membrane-associated biomarkers. For improved signal-to-background ratio and high tumor specificity, candidate markers should be selectively expressed on tumor cells while being absent on healthy tissue. Membrane Hsp70 has been found to fulfill these criteria exhibiting remarkable tumor specific targeting capabilities [7,8]. In the course of cancer treatment, standard regimens, such as radiotherapy or chemotherapy, have been shown to increase the membrane expression density of Hsp70 on tumor cells [9], promoting membrane Hsp70 activated tumor targeting in combination with standard therapies. Furthermore, an upregulated Hsp70 membrane density could be detected on relapse tumors and metastases, compared to primary tumors. In multiple studies, the malignancy of tumors is correlated with the Hsp70 status in the cytoplasm and on the plasma membrane [7,10]. For a specific *in vivo* tumor targeting mediated by membrane-associated Hsp70, we developed the Hsp70 membrane-specific antibody cmHsp70.1 [8,11]. To utilize the beneficial features of targeting membrane Hsp70 with the imaging capabilities of noble metals as a contrast agent, we developed a gold nanoparticle formulation, functionalized with cmHsp70.1 monoclonal antibody to target membrane-bound Hsp70 on tumor cells, *in vivo*. In previous studies we could demonstrate the rapid and specific binding, uptake and internalization of cmHsp70.1-AuNPs into tumor cells *in vitro*, leading to a high intracellular accumulation. Furthermore, following incubation of viable tumor cells with cmHsp70.1-AuNP, no toxicity was observed up to a concentration of 10 µg/ml [12].

2. Results

2.1 Functionalization of gold nanoparticles with cmHsp70.1

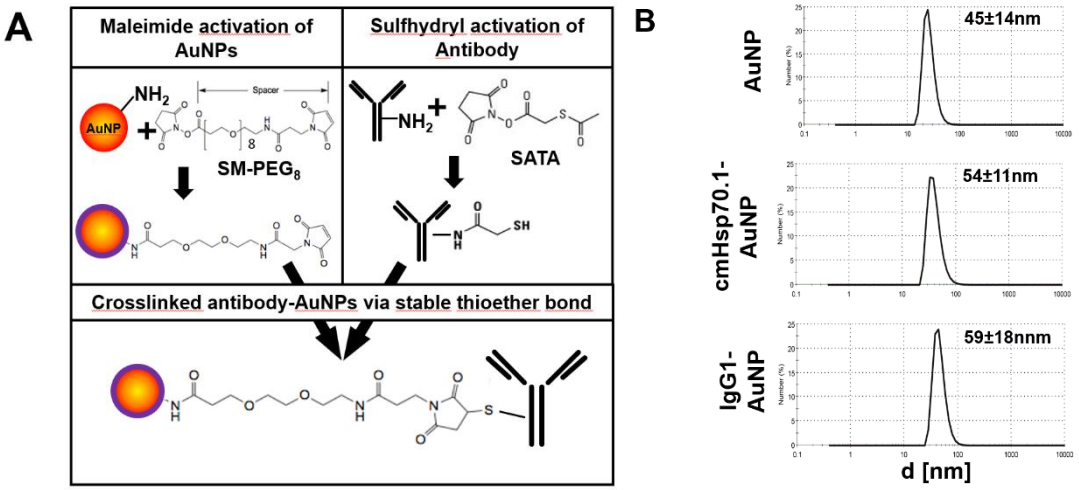

Figure 1. Antibody conjugation of gold nanoparticles and characterization. (A) Coupling reaction of maleimide-activated AuNP and sulfhydryl-activated monoclonal antibodies. (B) Size distribution of the differently functionalized AuNP, given in size by number-histograms.

Peer-reviewed version available at Cancers 2020, 12, 1331; doi:10.3390/cancers12051331

For the coupling of mouse IgG1 isotype- or cmHsp70.1 antibodies to gold nanoparticles, sulfhydryl groups were added to the N-terminal residue of cmHsp70.1mAb or mouse IgG1 control antibody using SATA. Amine residues at the gold nanoparticles (AuNP) were coupled to maleimide and further to a PEG spacer to facilitate steric flexibility of the antibodies (Figure 1A, top panel). A covalent cross-link of sulfhydryl-activated antibodies and maleimide-activated gold nanoparticles was established by coincubation at pH 6.5–7.5 (Figure 1A, bottom panel). The size of the mean hydrodynamic diameter of unconjugated gold nanoparticles (AuNP) was determined to 45±14 nm (Figure 1B, top panel). The size of cmHsp70.1 antibody (cmHsp70.1-AuNP)-conjugated AuNP was 54±11nm (Figure 1B, middle panel), 59±18 nm for IgG1 isotype-matched control antibody-conjugated gold nanoparticles (IgG1-AuNP) (Figure 1B, bottom panel). No self-aggregation was observed in aliquotes of the conjugated as well as the unconjugated gold nanoparticles in PBS at 37°C during 24 hours; After 4 weeks at 4°C, starting self-aggregation of the particles was observed. An exemplary size distribution histogram is given in Figure S1.

2.2 Uptake and internalization of functionalized AuNP in tumor cells, in vitro

To verify the binding capacities and the specific uptake of cmHsp70.1-AuNP in comparison to control NPs (AuNP, IgG1-AuNP) *in vitro*, we performed binding tests on viable, membrane Hsp70-positive tumor cells. To determine the density of the target antigen, the cell lines 4T1 and CT26 were analyzed for their membrane and cytosolic expression of Hsp70. The Hsp70 high expressing cell line 4T1 showed a membrane Hsp70-positive phenotype on 67±9%, whereas CT26 cells yielded a positivity of 43±6% of the cells (Figure 2A). For determination of the total Hsp70 density in the cell lines, an in-cell ELISA technique was established for cells grown in chamber slides. The Hsp70 mean signal intensity levels in 4T1 and CT26 cell lines were 150.11*10^3 ± 24.92*10^3 a.u. and 89,39*10^3 ± 17.19*10^3 a.u., respectively (Figure 2B). These data were verified by a sandwich-ELISA of cell lysates derived from 10*10^6 cells of each cell line, resulting in Hsp70 contents of 4.28±1.74 ng/ml and 1.17±0.72 ng/ml

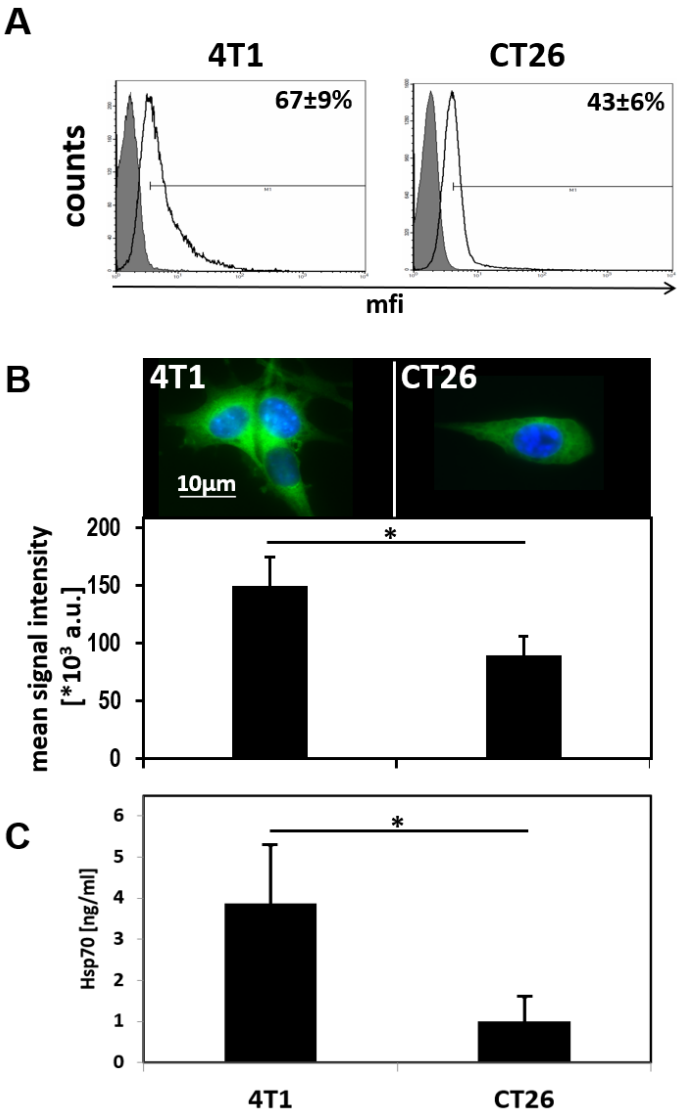

Figure 2. Quantification of Hsp70 in target tumor cell lines. (A) Plasma-membrane bound Hsp70 of 4T1 (left) and CT26 (right) cell lines, as determined by flow cytometry. (B) Quantitative staining of total Hsp70 in 4T1 and CT26 cells (upper panel) and quantification thereof (lower panel), as determined by in cell ELISA technique. (C) Quantification of total Hsp70 on whole cell lysates of 4T1 and CT26 cell lines, as determined by Hsp70 sandwich ELISA.

Preprints (www.preprints.org) | NOT PEER-REVIEWED | Posted: 17 April 2020 doi:10.20944/preprints202004.0297.v1

Peer-reviewed version available at Cancers 2020, 12, 1331; doi:10.3390/cancers12051331

for 4T1 and CT26 cells, respectively (Figure 2C). Subsequently, both cell lines were incubated with the three different types of AuNPs for 24 hours at 37°C, to mimic the uptake *in vivo*. In both cell lines, the content of gold nanoparticles was visualized by brightfield and electron microscopy (Figure 3). Compared to blank AuNP (Figure 3A, left panel) and IgG1-AuNP (Figure 3A, middle panel), which showed minor cytosolic uptake, cmHsp70.1-AuNP displayed the strongest accumulation in both, 4T1 and CT26 cells (Figure 3A, right panel). In Electron Microscopical imaging, the cmHsp70.1-AuNP have been found to accumulate in intracellular vesicles within the internalizing cells of both investigated cell lines after 24h of incubation. A representative image of cmHsp70.1-AuNPs in 4T1 cells is given in Figure 3B.

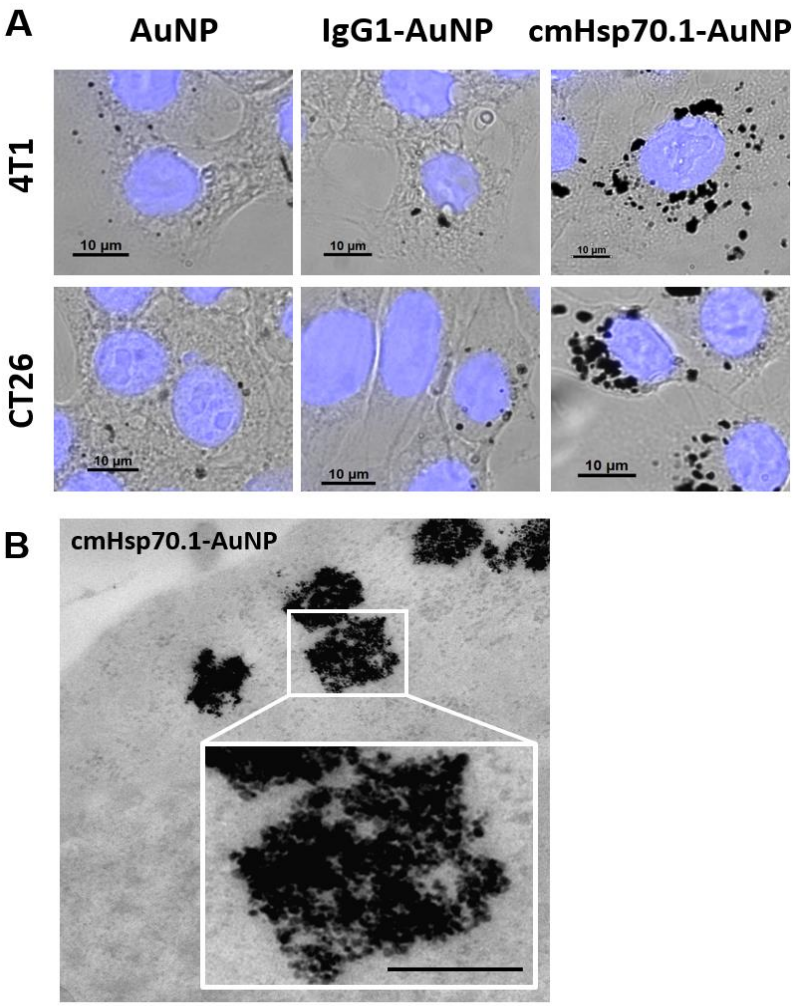

Figure 3. Uptake of AuNP in tumor cells. (A) Intracellular accumulation of blank AuNP (left), mouse IgG1 coupled AuNP (middle) and cmHsp70.1 functionalized AuNP (right) in 4T1 (upper panel) and CT26 (lower panel) cells. (B) TEM image of intracellular accumulations in 4T1 cells. Scale bar, 1 µm.

2.3 Accumulation of functionalized AuNP in tumors, in vivo

To investigate the specificity and sensitivity of Hsp70.1-conjugated AuNP to target tumors *in vivo*, syngenic tumor models in Balb/c mice were established. Animals were inoculated with orthotopic 4T1 and subcutaneous CT26 tumors, respectively. When tumor lesions reached a size of 200 mm^3, two times 2.5 mg of AuNP of each group (AuNP, IgG1-AuNP and cmHsp70.1-AuNP) were injected i.v. consecutively at an interval of 24 hours (Figure 4). 24 hours after the second injection, mice were euthanized and fixated. After fixation, mice were either imaged using spectral-CT or directly applied to histological analysis. In the following, organs and tumors of the animals were

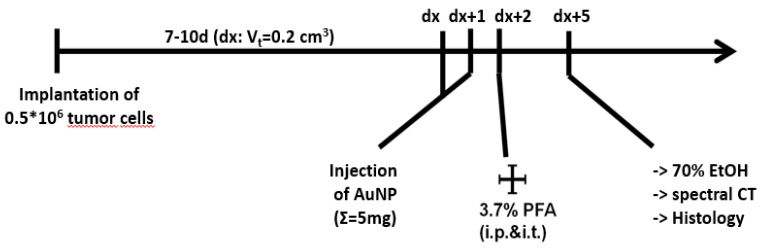

Figure 4. Timeline of the *in vivo* experiments.

Peer-reviewed version available at Cancers 2020, 12, 1331; doi:10.3390/cancers12051331

histologically analyzed. In parallel, single cell suspension of tumors of both models have been analyzed for the plasma membrane Hsp70 status. To characterize the tumor models regarding the main features which determine the accumulation of molecular functionalized contrast agents *in vivo*, tumors were histologically analyzed for the target antigen content (Hsp70) in the cytoplasm as well as on the plasma membrane. Their vascularization status (CD31) and the presence of tumor infiltrating macrophages (F4/80) have been investigated as well. Both tumor types, 4T1 o.t. and CT26 s.c., displayed similar vascularization and infiltration of macrophages, indicating comparable effects on the NP input through these routes. Immunohistological Hsp70 staining revealed strong expression in both tumor models, featuring cytosolic as well as nuclear Hsp70 expression. However, 4T1 tumors showed a more patterned architecture of the Hsp70 density. To investigate the membrane Hsp70 status of the tumors *in vivo*, a single cell suspension of the freshly dissected tumors was investigated. With 76±7% and 67±13% membrane Hsp70 positive viable tumor cells, 4T1 tumors and CT26 tumors, respectively, showed slightly higher expression, compared to the *in vitro* cultured cells. However, the increased width of the cytometric data, as given in histograms, indicates increased heterogeneity in the membrane Hsp70 expression pattern in *in vivo* grown tumors. (Figure 5).

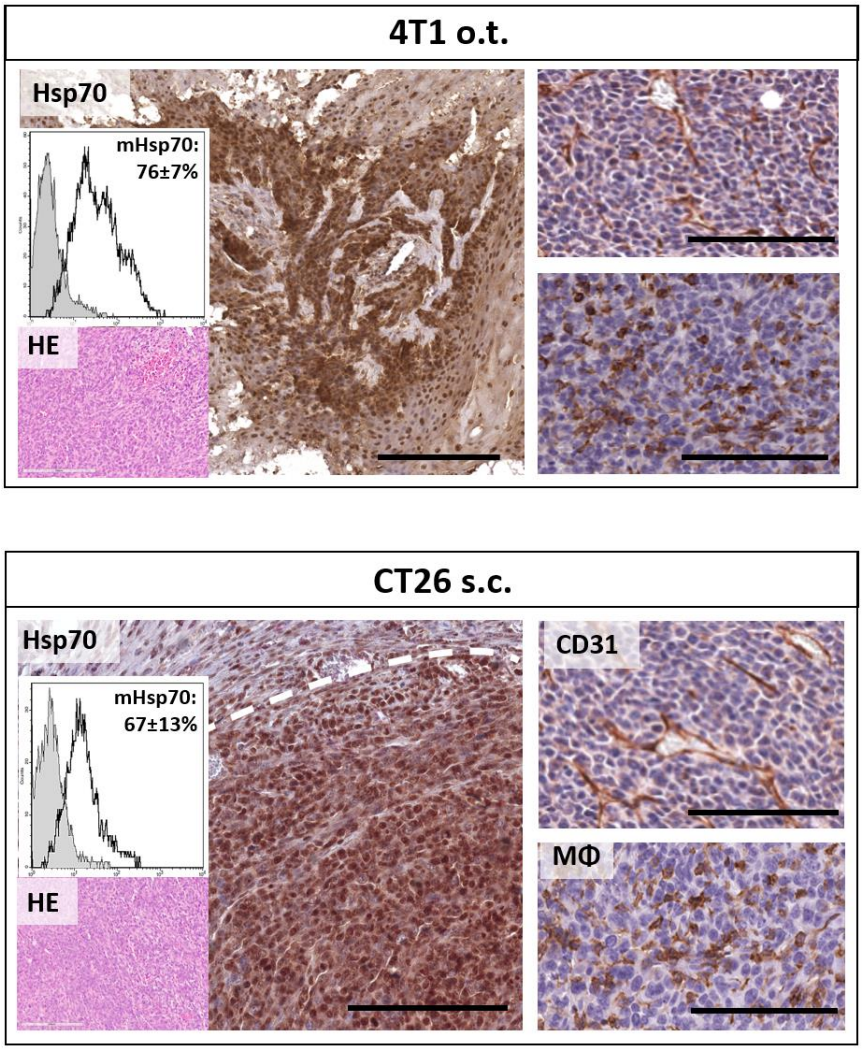

Figure 5. Hsp70.1 tumor characterization. Orthotopical 4T1 (upper panel) and subcutaneous CT26 (lower panel) tumors were analyzed with regard to membrane (FACS, upper inlay) - and overall (IHC) Hsp70 expression, as well as their content of vessels (IHC, CD31) and the infiltration of macrophages (IHC, F4/80). H&E was used as overview stain (lower inlay). Scale bars, 200µm (Hsp70), 100µm (CD31, MΦ).

To investigate the feasibility of cmHsp70.1-AuNPs as a contrast agent, in a next step we analyzed a first cohort of tumor bearing mice by spectral CT. In both tumor models, we additionally investigated the biodistribution of the differently functionalized AuNP in tumors and organs. Spectral CT technique allows for the simultaneous detection of AuNPs and the anatomical structures due to a combination of K-edge analysis and conventional CT. For this pilot study, mice with CT26 tumors underwent spectral CT imaging post mortem. Each mouse had received one type of AuNP. Interestingly, in all animals we were able to detect AuNP in the tumors. In any observed tumor, the highest density of nanoparticles was traced

Peer-reviewed version available at Cancers 2020, 12, 1331; doi:10.3390/cancers12051331

back in the tumor periphery. The mouse treated with IgG1-AuNP i.v. presented the lowest content of AuNP in the tumor (3.3 µg Au/mm³ tumor) with a low accumulation of particles within the tumor center (Figure 6A, B). In mice treated with unconjugated AuNP, high amounts of NP were mainly found at the periphery of the tumor (4.3 µg Au/mm³ tumor), with considerably less AuNP content in the tumor center. In comparison, the highest content of AuNP was found in mice injected with cmHsp70.1-AuNP i.v. (4.4 µg Au/mm³ tumor). In this group, the NP were located in the tumor periphery as well as in the tumor center (Figure 6C, D). In spectral CT based biodistribution analysis, the content of Nanoparticles was also investigated in the organs of the mice. We detected high accumulation in the spleen, and to a lesser extent in the liver and lung. The other organs did not exhibit concentrations high enough to generate a signal in spectral CT measurements. The gold signal of spectral CT measurements was further verified by histological analysis of the tumors (Figure 7). Sections were treated with silver enhancement to visualize the gold nanoparticles by light microscopy (Figure 7A). As revealed by spectral-CT, histological analysis confirmed the varying intratumoral distribution of the three groups of AuNP. In tumors of mice which were treated with cmHsp70.1-AuNP, a more homologous distribution of NP was observed throughout the tumor volume, compared to the blank AuNP or IgG1-AuNP. Notably, the enrichment of AuNP following i.v. injection of blank AuNP was to a large extent due to introduction by F4/80 positive cells of the monocyte / macrophage lineage, which phagocytosed the non-camouflaged nanoparticles and subsequently located into the tumor periphery (Figure 7B, left). In contrast, next to the payload introduction via tumor-infiltrating macrophages, cmHsp70.1-AuNP were also found in large amounts in F4/80 negative cells of the tumor. Consequently, an extended accumulation of the cmHsp70.1-AuNP was also detected in the tumor center region, which showed less content of AuNP containing, recently infiltrated macrophages (Figure 7B, right). IgG1-AuNP showed the lowest accumulation in all regions of the tumor. These NP, besides their lack of targeting capacity, exhibited equal biocompatibility to cmHsp70.1-AuNP, due to the coating by murine antibodies of the isotype IgG1. Consequently, this type of NP resultet in the lowest intratumoral accumulation yield.

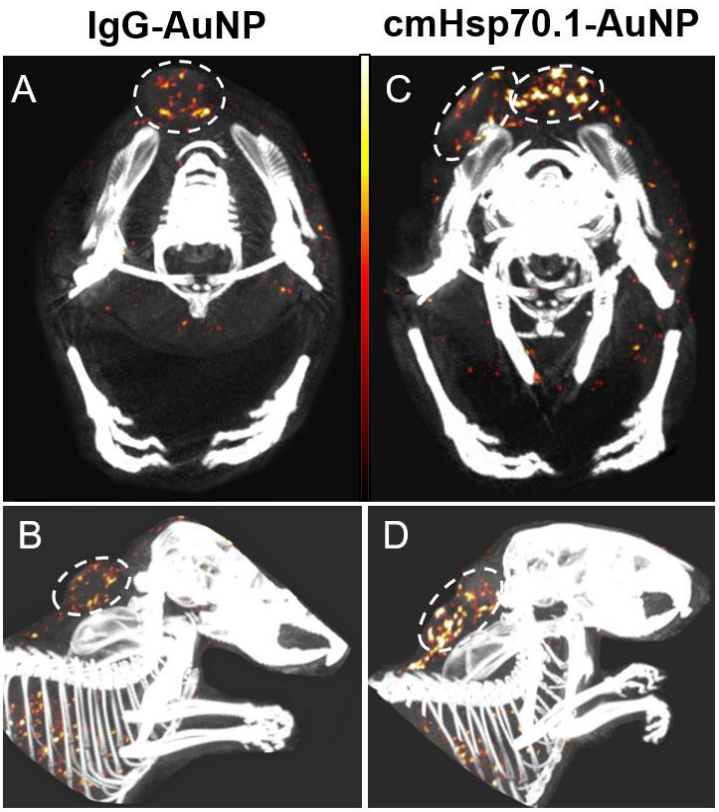

Figure 6. Tumor detection using spectral-CT. Upper Row: axial view, bottom row: sagital view. AuNP amounts (mg/ml) are pseudo-coloured from black (6.5 mg/ml) over red (10 mg/ml) to white (13.5 mg/ml).

Preprints (www.preprints.org) | NOT PEER-REVIEWED | Posted: 17 April 2020 doi:10.20944/preprints202004.0297.v1

Peer-reviewed version available at Cancers 2020, 12, 1331; doi:10.3390/cancers12051331

To obtain the *in vivo* biodistribution characteristics of cmHsp70.1-AuNP featuring a diameter of about 50 nm, 24 hours following systemic application, we analyzed silver enhanced sections of tumors, liver, spleen, kidneys, heart, lungs and intestines of tumor bearing Balb/c mice (Figure 8).

For improved accuracy of the analysis, we used a machine-learning approach. The algorithm for the analysis of sectrions was trained on 28 slides in total and was applied for the analysis of 13 slides. In comparison to the organs, the highest accumulation of cmHsp70.1-AuNP was found in the tumors, with $85.98*10^3 \pm 4.94*10^3$ positive pixel per mm^2, which equals to 2.7% positive pixels per section (Figure 8B). In accordance to findings of Yang et al [13], the majority of the NP accumulated in spleen ($14.04*10^3 \pm 1.37*10^3$ pixel/mm^2) (2.13% signal/section), liver ($13.34*10^3 \pm 0.7*10^3$ pixel/mm^2) (0.11% signal/section) and intestine ($9.48*10^3 \pm 1.37*10^3$ pixel/mm^2) (0.34% signal/section), followed by lungs ($6.28*10^3 \pm 1.30*10^3$ pixel/mm^2) (0.09% signal/section). In muscle, as represented by heart tissue, the accumulation of AuNP was below detection limit. Kidney was rarely affected, indicating an enterohepatic secretion of the AuNP. Next to the analysis of overall entry of AuNP in the organs and tumors, we utilized the machine-learning approach to analyze the size distribution of nanoparticle agglumeration within the

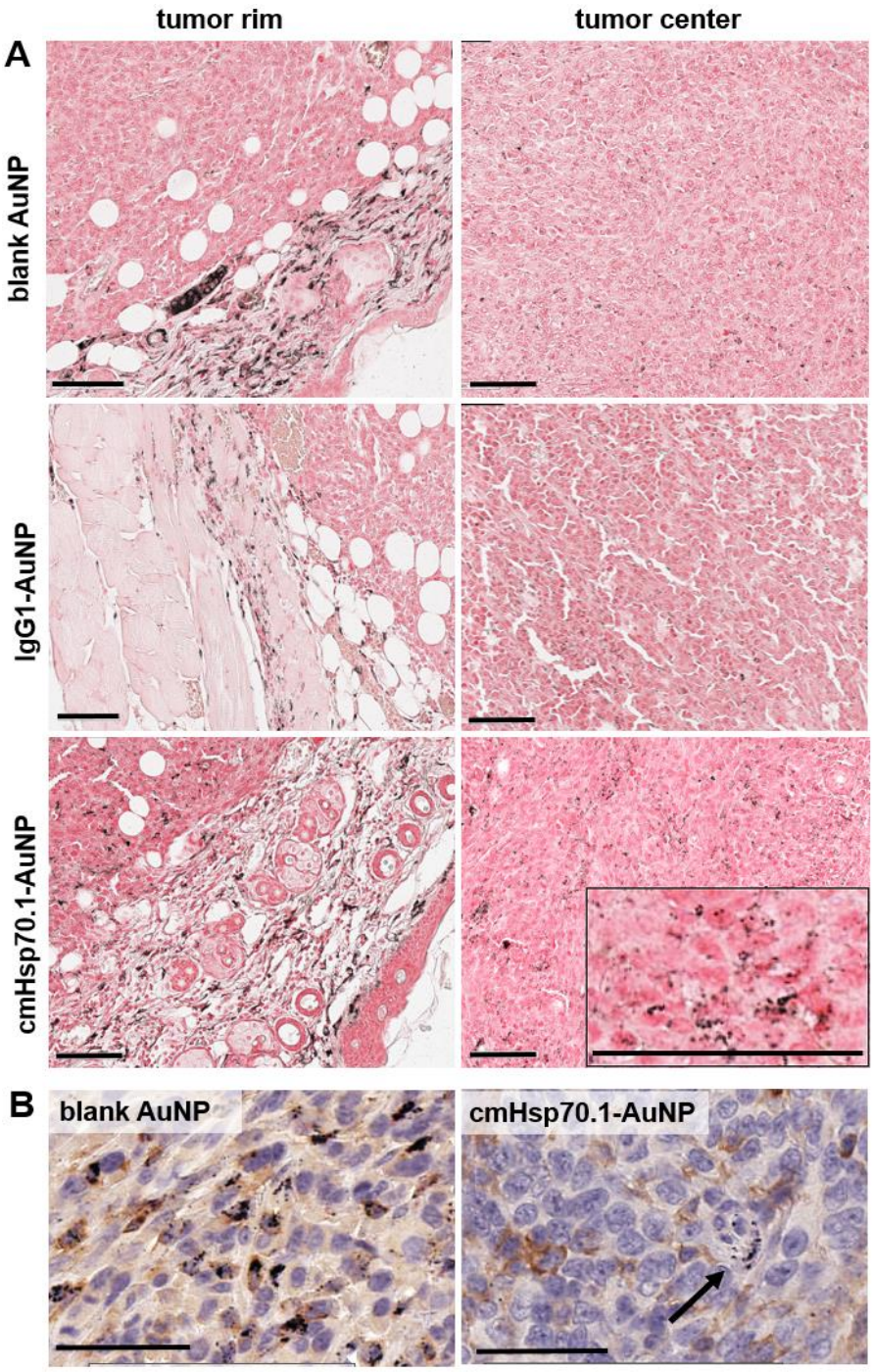

Figure 7. AuNP uptake and distribution in CT26 tumors. (A) Silver enhancement of AuNP. Upper row: blank AuNP, middle row: IgG1-AuNP, bottom row: cmHsp70.1-AuNP. Left: ROI at tumor rim area, right: ROI set to tumor center. Scale bars, 100 µm. (B) double staining of Macrophages (F4/80, brown) and silver enhancement of AuNP (black). Arrow: single-positive cells for AuNP. Scale bars: 5 µm.

Preprints (www.preprints.org) | NOT PEER-REVIEWED | Posted: 17 April 2020 doi:10.20944/preprints202004.0297.v1

Peer-reviewed version available at Cancers 2020, 12, 1331; doi:10.3390/cancers12051331

organs. The majority of positively stained events in liver and spleen resultet in a size range up to 10µm. Accumulation of events in this size range might be suggested to be due to incorporation of the AuNP by Macrophages and Kupffer cells, as indicated also in Figure 7B. The majority of AuNP in kidney, lung and intestine yielded in agglumerates of about 1µm in size. In the tumor, Hsp70.1-AuNP spots of 25µm² were dominant followed by spots of 1µm² (Figure 8C). As tumor-associated macrophages exhibit large cytoplasmatic volumes, the accumulation of AuNP above 10µm² suggest the appearence within this cell type. However, aggregates of 1µm² size point to tumor cells with smaller cytoplasmic space, as tumor cells. This finding is also supported by microscopical analysis of *in vitro* grown tumor cells with the majority of NP accumulating in cellular organelles of about 1µm, following endocytosis (Figure 3).

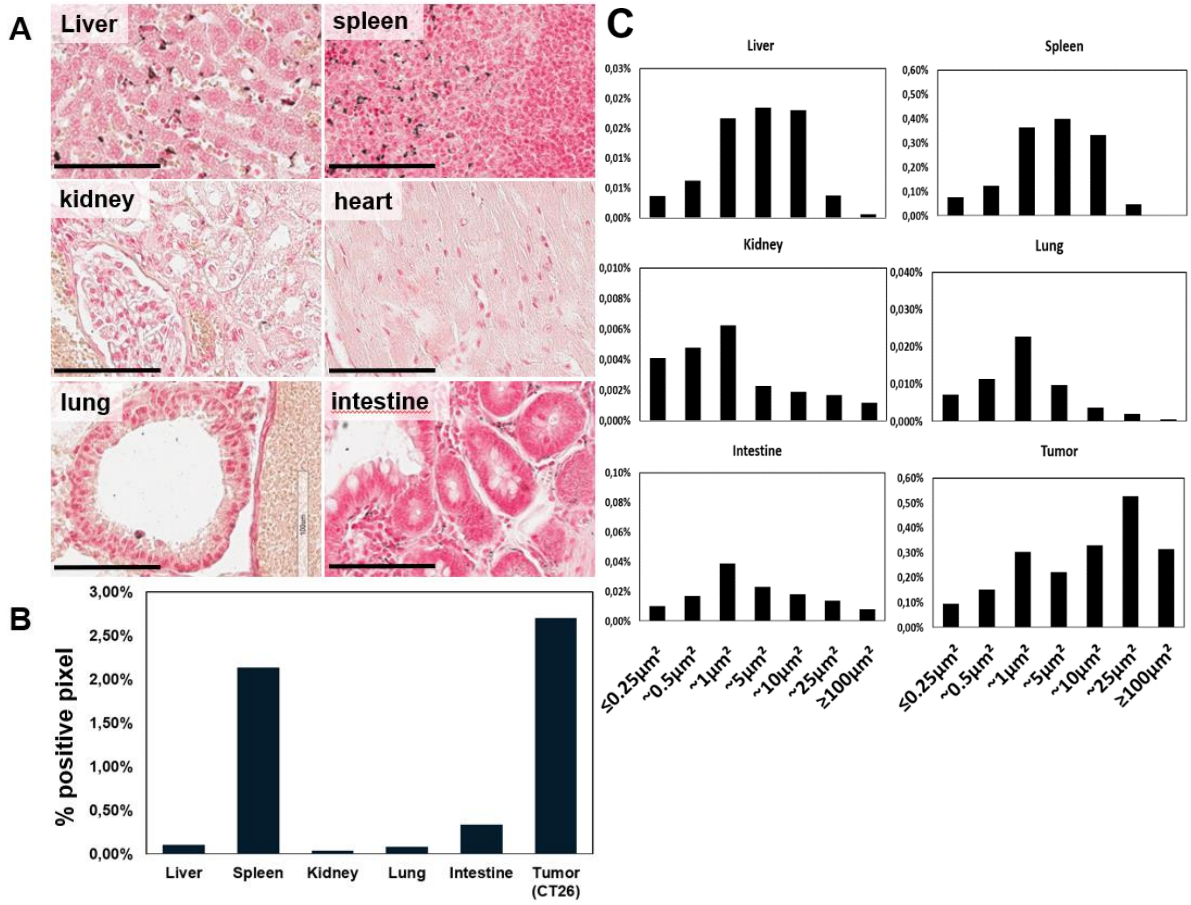

Figure 8. Biodistribution of cmHsp70.1-AuNP. (A) Silver enhancement staining of liver, spleen, kidney, heart, lung and intestine. Scale bar, 100 µm. (B) Pixel analysis of silver enhancement stainings in tumors and organs, given in positive pixel/mm² tissue. (C) size distribution of silver enhanced cmHsp70.1-AuNP signals in different organs, following i.v. injection.

3. Discussion

The discovery of suitable contrast agents for the visualization of tumors is one of the most important areas in clinical research. In tumor imaging, CT imaging is the most commonly used technique featuring fast scanning speed with high spatial resolution of a large portion of the body. Functional molecular imaging can be accomplished with positron-electron-tomography (PET), often used in combination with CT. However, certain limitations affect the quality of tumor visualization. PET imaging using ^{18}F-FDG is highly dependent on a high tumor cell metabolism compared to the surrounding normal tissue. Furthermore, PET tracer need to exert ionizing effects, which in turn increases the patient's risk to accumulate DNA mutations. An approach to overcome the limiting effects of PET/CT led to the development of spectral-CT analyzers [5,14], which use the k-edge

Peer-reviewed version available at Cancers 2020, 12, 1331; doi:10.3390/cancers12051331

discrimination of elements allowing for their specific identification inside the body [15]. Another advantage of the spectral segmentation is the possibility to utilize multiple contrast agents within one imaging session which reduces x-ray exposition of the patient.

One further limitation is the spacial detection limit leading to a potential miss of small lesions. Therefore, the usage of tumor-specific markers is beneficial.

Herein, the major stress-inducible member of the HSP70 family, Hsp70 (HspA1A) was used as a target for the tumor-specific uptake of functionalized gold nanoparticles in different tumor entities. Hsp70 is expressed on a variety of tumor entities, whereas normal cells lack an Hsp70 membrane expression [8]. In previous studies, we observed that membrane associated Hsp70 is rapidly internalized, and thereby mediating an efficient uptake of Hsp70 binding probes into the cytoplasm, such as fluorescence-labeled cmHsp70.1 antibody [11] and tumor penetrating peptide (TPP) [16,17]. Since the binding epitope of cmHsp70.1 antibody is identical in mouse and human tumor cells [8], murine CT26 colon and mammary 4T1 tumor cell lines were used in the present study.

The application of gold nanoparticles for imaging *in vivo* is a promising new approach in the field of *in vivo* imaging [6,18,19]. The uptake of antibody-conjugated nanoparticles into tumor cells is dependent on different factors. The expression density of receptors, which are expressed on the target cells, the distribution of the target epitopes throughout the cells [20], the affinity of the tracer to the membrane epitope and the speed of internalization [16,21].

In order to monitor the quality of functionalized gold nanoparticles *in vitro* and *in vivo*, different imaging modalities were applied. Dynamic light scattering is a widely used technique to determine the hydrodynamic diameter of AuNP in the nm–µm range.

Finally, the quantification of gold nanoparticles within tumor cells is of relevance to estimate the amount of nanoparticles that is necessary for noninvasive *in vivo* imaging of tumors in mice and humans as well as for their use as therapeutic agent. In our *in vivo*/*ex vivo* setup, we were able to detect aggregates of gold nanoparticles in tumors and organs in perinuclear areas of around 1–2 µm in diameter, as well as larger aggregates of around 25µm in diameter. The here presented machine-learning approach has proven to be beneficial for the analysis of AuNP distribution. Next to calculating the quantity of gold signal within tumor and organs, we were able to separate the signal into groups which allows for an easy analysis of AuNP within different cell types. This is important for precise prediction of biodistribution and possible toxicity of AuNP.

Toxic side effects of gold nanoparticles following i.v. application was investigated in previous studies. No negative side effects such as loss in body weight or organic dysfunctions were observed in these experiments up to a concentration of 500 µg/mL [22]. Concordantly, in the *in vivo* experiments of this study we did not observe any sign of toxicity at the injected concentration of 5 mg AuNP per mouse. However, additional pharmacological and toxicological studies are needed to prove safety.

On the basis of the specific and quantitative uptake of cmHsp70.1-AuNP in Hsp70-positive tumor cells and its imaging properties, our approach hints to a possible beneficial use in radiation therapy. Numerous studies have reported on the radiation enhancing effect that gold nanoparticles within the tumor tissue [23,24].

A promising finding was achieved for radiotherapy enhancement of gold nanoparticles in preclinical mammary carcinoma studies. The results showed an 86% 1-year survival for an combinatorial therapy of irradiation in presence of NPs, compared to 20% for radiotherapy alone [25]. Probable mechanisms involved in radiosensitization are, besides changes in the cell cycle or an elevated reactive oxygen species, the production and the release of secondary Auger electrons by gold in very close proximity to the nucleus [24].

In summary, we demonstrate that the functionalization of gold nanoparticles with cmHsp70.1 antibody is a highly promising approach for *in vivo* tumor targeting. In these preclinical studies, the accumulation of the investigated tumors was sufficient for visualization in spectral-CT allowing for 3D reconstructions and quantifications.

4. Materials and Methods

Antibody coupling of Gold Nanoparticles

Coupling of Hsp70-specific antibody (cmHsp70.1, multimmune, Germany) or an isotype-matched control IgG1 antibody (Sigma Aldrich, St. Luis, Mo, USA) to gold nanoparticles (Nanopartz, Loveland, CO, USA) was done as described before [12]. Briefly, PEG-amine coated spherical gold nanoparticles of 30 nm diameter were maleimide activated (Pierce, Thermo Fischer Scientific, Rockford, IL, USA) and incubated over night with sulfhydryl-activated antibodies. Vacant binding sites were blocked with bovine serum albumin (BSA) (Sigma Aldrich, St. Louis, MO, USA). Antibody-coupled gold nanoparticles or BSA-blocked control gold nanoparticles were analyzed and used for experiments within 24 hours. Nanoparticles were analyzed (size, aggregation) by dynamic light scattering (Zetasizer NanoS, Malvern Instruments, Malvern, UK). Measurements were done in triplets and mean values calculated.

Characterization of AuNP

For coupling, spherical gold nanoparticles with a diameter of 30 nm were used (Nanopartz, Loveland, CO, USA). After washing of unbound antibodies, vacant binding sites on the gold nanoparticles were saturated by bovine serum albumin (Sigma-Aldrich, St Louis, MO, USA). Antibody-conjugated gold nanoparticles or only bovine serum albumin-blocked negative control AuNP were used for experiments directly after coupling. For characterization of the nanoparticles and checking for aggregation, particles were analyzed for their size by dynamic light scattering (Zetasizer NanoS; Malvern Instruments, Malvern, UK). Only nanoparticles with a single peak around 40 nm were used for experiments.

Cell culture

Murine colon carcinoma cell line CT26 (CT26.WT; American type culture collection (ATCC) #CRL-2638) and the mouse mammary carcinoma cell line 4T1 (ATCC #CRL-2539) were cultured in Roswell Park Memorial Institute 1640 medium supplemented with 10% (v/v) heat-inactivated fetal calf serum, 2 mM l-glutamine, 1 mM sodium pyruvate and antibiotics (100 IU/mL penicillin and 100 µg/mL streptomycin). Cells were incubated at 37°C in 95% humidity and 5% (v/v) CO_2 and cultivated twice a week.

Assessment of Hsp70 content of the tumor cells

The Hsp70 membrane phenotype of the cells was assessed by flow cytometry. Single cell suspension of tumor cell lines was incubated with fluorescein-isothiocyanate (FITC)-conjugated cmHsp70.1 mAb for 30min on ice. As controls, conjugation of an IgG1 isotype-matched antibody was done. After washing and adding propidium-iodide (PI) for life and dead discrimination, binding of antibodies was measured using a FACSCalibur instrument (BD Biosciences). Data were analyzed using CellQuest Pro software. Only PI negative, viable cells were analyzed. To determine the membrane Hsp70 status of tumors grown *in vivo*, single cell suspension of freshly dissected tumors was generated by combined chopping and trypsin treatment of the tumors. Here, anti-mouse CD45 APC antibody was added to cmHsp70.1-FITC to distinguish tumor cells from mononuclear blood cells and infiltrated macrophages.

In cell ELISA was performed as described before [16]. Briefly, cells grown in chamber slides were fixed with DAKO Fix & Perm kit, cellular membranes were permeabilized and incubated with cmHsp70.1-FITC antibody. Following microscopy with comparable settings, quantification of fluorescence signal was determined on the mean signal intensity values by ImageJ image analysis software.

Quantification of the Hsp70 content was confirmed by an Hsp70 sandwich ELISA as described elsewhere [26]. Shortly, after determination of the cell count, cells were lysed by incubation in Tris-HCl based buffer containing 1% Triton-X100 and SDS. After centrifugation, the Hsp70 concentration in the supernatant was measured by total Hsp70 ELISA kit (R&D systems, USA) as described by the manufacturer. Each supernatant sample was measured in duplicates.

Peer-reviewed version available at Cancers 2020, 12, 1331; doi:10.3390/cancers12051331

Animals

All animal procedures and their care were conducted in conformity with national and international guidelines (EU 2010/63) with approval from the local authorities of the Government of Upper Bavaria and St. Petersburg, Russia and supervised by respective Animal Care and Use Committees. Animals were housed in standard animal rooms in individually ventilated cage systems (IVS Techniplast) under specific pathogen-free conditions with free access to water and standard laboratory chow ad libitum. In total, 6 female Balb/c mice (aged 10-14 weeks, Charles River Laboratories, Sulzfeld, Germany) were used. Induction of subcutaneous tumors was done under inhalation anesthesia (1.8% isoflurane with medical O_2) by injection of $5*10^5$ CT26 cells subcutaneously in the neck area, or $5*10^5$ 4T1 cells orthotopically in the 4th mammary fat pad. When tumors reached a size of 200 mm^3, gold nanoparticles were intravenously injected using standard procedures. In total, 5 mg unconjugated, IgG1- or cmHsp70.1-conjugated gold nanoparticles, suspended in phosphate buffered saline, were injected in a consecutive pattern of two times 2.5 mg per day within 24h. Another 24 hours after the second application, mice were euthanized under deep anesthesia, fixed in 4% neutral-buffered formalin for 5 days and stored in 70% ethanol for further analysis.

Bright field Microscopy

For light microscopy, cells were grown in 8-well chamber slides (NUNC-Nalgene; Thermo Fisher Scientific) at a concentration of 10,000 per well. Upon adherence, cells were incubated with gold nanoparticles at a non-toxic concentration of 1 µg/mL. Cellular uptake of AuNP or quantum dots of the same size were analyzed with a Zeiss Observer Z1.

Transmission Electron Microscopy

Cells were co-incubated with functionalized and non-conjugated nanoparticles (at a concentration 100 ug/ml) for 24 hours. Following incubation cells were washed with PBS, fixed for 1 hour at 4 C in 2.5% glutaraldehyde in 0.1 M cacodylate buffer (pH=7.4), postfixed in 1% aqueous OsO4 (for 1 hour), dehydrated, and embedded in Araldite-Epon mixture. Sections were assessed employing Zeiss Libra 120 electron microscope (Carl Zeiss, Germany).

Histology and Immunohistochemistry

Tumors and organs were either dissected following whole-body fixation of mice, or fixed in 3.7% neutral-buffered formaldehyde and embedded in paraffin. 2µm sections of the organs and tumors were prepared, and the morphology visualized by standard H&E staining. For immunohistochemistry the activity of the endogenous peroxidase was blocked with 1% hydrogen peroxide and 0.1% sodium azide. After antigen retrieval in citric acid buffer (pH 6) at 100°C, sections were incubated with anti Hsp70 antibody cmHsp70.1, followed by HRP-labelled secondary rabbit anti-mouse antibody (Dako, Germany). Diaminobenzidine (Dako) was used as a chromogen. Sections were counterstained with 1% Mayer's hematoxylin. To visualize the gold-nanoparticles by light microscopy, silver-enhancement staining was used according to the manufacturers´ protocol (Sigma-Aldrich, Darmstadt, Germany), followed by counterstaining of the nuclei with 0.1% Nuclear Fast Red solution. Slides were digitalized with a digital slide scanner (AT2, Leica, Germany).

Spectral-CT imaging and image acquisition

Spectral CT images were acquired at a Philips spectral CT scanner, as described before [14]. Briefly, a preclinical spectral photon-counting CT system (Philips Healthcare, Haifa, Israel) was used to obtain axial scans over 360° at a beam voltage of 100kVp. For optimal discrimination of the signals of AuNP, a threshold was set at the k-edge energy of gold.

Spectral CT image-based Gold quantification

Osirix® MD v10.0.5 software (Pixmeo SARL, Bern, Switzerland) was used for analysis. Mean background was measured from several ROIs in the spleen. Gold amounts were calculated over the whole tumor volume (µg gold/mm^3).

Deep learning-based quantification of AuNP histology

The bio-distribution of silver-stained AuNP in histological slides was assessed with the help of a deep neural network. Regions of interest in each slide were defined via manual delineation. Slides were subdivided into smaller, slightly overlapping patches of 1,000 x 1,000 pixels to meet memory constraints. In a first preliminary step, AuNP concentrations were segmented with the help of color-channel-specific dynamic thresholding and morphological operations (opening and closing with fixed kernels). Parameters were manually tuned to optimize results for the majority of slides. In a second step, the best resulting binary masks were manually selected and partially manually corrected. In a third step, a deep neural network was trained to segment AuNP concentrations on this basis. In a final step, the trained network was used to derive segmentations of AuNP concentrations for all slide patches. A k-fold rotation of data splits was applied so that the network yields segmentations on data samples that were not used for training, ensuring that the segmentation represents the result of the learned task rather than replicating

the threshold-derived training data. This procedure yielded substantially more accurate and consistent segmentations of AuNP concentrations as compared to the preliminary thresholding procedure. Subsequent re-concatenation of slightly overlapping slide patches ruled out boundary effects and double-counting. In a post-processing step, all individual AuNP concentrations were identified via connected-component analysis, allowing to assess their individual sizes.

The deep neural network follows a U-net like architecture and consists of 4 levels of en- and decoding units. Each layer of encoding units doubles the number of feature channels, starting from 16 and ending at 265 at the deepest level. The network was trained for 10 epochs on a training set of ca. 5,000 patches. Details of architecture, implementation, and training procedure follow a previously described protocol [27].

5. Conclusions

Herein, we show that the visualization of tumor cells with gold nanoparticles by addressing membrane Hsp70 is feasible. We present data showing a superior uptake of cmHsp70.1 antibody-conjugated gold nanoparticles in Hsp70 membrane-positive tumor cells. Inside the tumor cells, these particles accumulated in the perinuclear region within 24 hours. The Hsp70 specificity was shown since unconjugated nanoparticles and nanoparticles conjugated with an irrelevant control antibody were not taken up into Hsp70 membrane-positive tumor cells. Furthermore, Hsp70 knockout tumor cells that do not express Hsp70 in the cytosol and on the plasmamembrane showed no uptake of the cmHsp70.1-conjugated nanoparticles. Quantification of the internalized cmHsp70.1-conjugated gold nanoparticles reveals a high sensitivity for the detection of single cells. Experiments are ongoing to study the capability of cmHsp70.1 antibody-conjugated gold nanoparticles for spectral CT imaging of further Hsp70 membrane-positive tumor models and whether these nanoparticles can be used for therapeutic approaches. In the future, these antibody-conjugated gold nanoparticles may be useful for spectral computed tomography of tumors for diagnostic purposes and radiotherapeutic interventions.

Supplementary Materials: The following are available online at www.mdpi.com/xxx/s1, Figure S1:

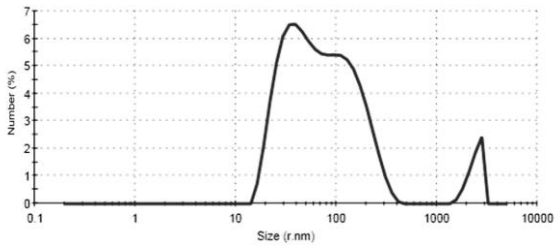

Figure S1. Size distribution of cmHsp70.1-AuNP after 2 weeks at 4°C. Size distribution is given in size by number histogram.

Author Contributions:

S. Stangl, M.A. Kimm and G. Multhoff designed the study. S. Stangl, M.A. Kimm, R. Proksa, M. Shevtsov, C. Werner, W. Sievert, Wu Zhiyuan, Olga Bystrova and Marina Martynova were responsible for data acquisition. Analysis and interpretation of data was performed by S. Stangl, M.A. Kimm, O. Schoppe, M. Shevtsov, C. Werner, W. Sievert, B. Menze and G. Multhoff. All authors were involved in drafting the article or revising it critically for important intellectual content and all authors approved the final version to be published.

Funding:

The study was supported by the Russian Foundation for Basic Research (RFBR) according to the research project №20-38-70039 and DFG grant (SFB824/3, STA1520/1-1; ME 3718/5-1), Technische Universität München (TUM) within the DFG funding program Open Access Publishing. Additional financial support was provided by TaGoNaX DFG project №336532926.

Conflicts of Interest:

The authors declare no conflict of interest.

References

1. Vanderstraeten, B.; Duthoy, W.; De Gersem, W.; De Neve, W.; Thierens, H. [18F]fluoro-deoxy-glucose positron emission tomography ([18F]FDG-PET) voxel intensity-based intensity-modulated radiation therapy (IMRT) for head and neck cancer. *Radiotherapy and oncology : journal of the European Society for Therapeutic Radiology and Oncology* **2006**, *79*, 249-258, doi:10.1016/j.radonc.2006.03.003.
2. Bal, H.; Guerin, L.; Casey, M.E.; Conti, M.; Eriksson, L.; Michel, C.; Fanti, S.; Pettinato, C.; Adler, S.; Choyke, P. Improving PET spatial resolution and detectability for prostate cancer imaging. *Physics in medicine and biology* **2014**, *59*, 4411-4426, doi:10.1088/0031-9155/59/15/4411.
3. Cormode, D.P.; Naha, P.C.; Fayad, Z.A. Nanoparticle contrast agents for computed tomography: a focus on micelles. *Contrast media & molecular imaging* **2014**, *9*, 37-52, doi:10.1002/cmmi.1551.
4. Chen, W.H.; Chen, J.X.; Cheng, H.; Chen, C.S.; Yang, J.; Xu, X.D.; Wang, Y.; Zhuo, R.X.; Zhang, X.Z. A new anti-cancer strategy of damaging mitochondria by pro-apoptotic peptide functionalized gold nanoparticles. *Chemical communications* **2013**, *49*, 6403-6405, doi:10.1039/c3cc43283a.
5. Cormode, D.P.; Roessl, E.; Thran, A.; Skajaa, T.; Gordon, R.E.; Schlomka, J.P.; Fuster, V.; Fisher, E.A.; Mulder, W.J.; Proksa, R., et al. Atherosclerotic plaque composition: analysis with multicolor CT and targeted gold nanoparticles. *Radiology* **2010**, *256*, 774-782, doi:10.1148/radiol.10092473.

6. Shevtsov, M.; Zhou, Y.; Khachatryan, W.; Multhoff, G.; Gao, H. Recent Advances in Gold Nanoformulations for Cancer Therapy. *Curr Drug Metab* **2018**, *19*, 768-780, doi:10.2174/1389200219666180611080736.
7. Sherman, M.; Multhoff, G. Heat shock proteins in cancer. *Annals of the New York Academy of Sciences* **2007**, *1113*, 192-201, doi:10.1196/annals.1391.030.
8. Stangl, S.; Gehrmann, M.; Riegger, J.; Kuhs, K.; Riederer, I.; Sievert, W.; Hube, K.; Mocikat, R.; Dressel, R.; Kremmer, E., et al. Targeting membrane heat-shock protein 70 (Hsp70) on tumors by cmHsp70.1 antibody. *Proceedings of the National Academy of Sciences of the United States of America* **2011**, *108*, 733-738, doi:10.1073/pnas.1016065108.
9. Gehrmann, M.; Radons, J.; Molls, M.; Multhoff, G. The therapeutic implications of clinically applied modifiers of heat shock protein 70 (Hsp70) expression by tumor cells. *Cell stress & chaperones* **2008**, *13*, 1-10, doi:10.1007/s12192-007-0006-0.
10. Stangl, S.; Tontcheva, N.; Sievert, W.; Shevtsov, M.; Niu, M.; Schmid, T.E.; Pigorsch, S.; Combs, S.E.; Haller, B.; Balermpas, P., et al. Heat shock protein 70 and tumor-infiltrating NK cells as prognostic indicators for patients with squamous cell carcinoma of the head and neck after radiochemotherapy: A multicentre retrospective study of the German Cancer Consortium Radiation Oncology Group (DKTK-ROG). *International journal of cancer* **2018**, *142*, 1911-1925, doi:10.1002/ijc.31213.
11. Stangl, S.; Gehrmann, M.; Dressel, R.; Alves, F.; Dullin, C.; Themelis, G.; Ntziachristos, V.; Staeblein, E.; Walch, A.; Winkelmann, I., et al. In vivo imaging of CT26 mouse tumours by using cmHsp70.1 monoclonal antibody. *J Cell Mol Med* **2011**, *15*, 874-887, doi:10.1111/j.1582-4934.2010.01067.x.
12. Gehrmann, M.K.; Kimm, M.A.; Stangl, S.; Schmid, T.E.; Noel, P.B.; Rummeny, E.J.; Multhoff, G. Imaging of Hsp70-positive tumors with cmHsp70.1 antibody-conjugated gold nanoparticles. *International journal of nanomedicine* **2015**, *10*, 5687-5700, doi:10.2147/IJN.S87174.
13. Yang, L.; Kuang, H.; Zhang, W.; Aguilar, Z.P.; Wei, H.; Xu, H. Comparisons of the biodistribution and toxicological examinations after repeated intravenous administration of silver and gold nanoparticles in mice. *Scientific reports* **2017**, *7*, 3303, doi:10.1038/s41598-017-03015-1.
14. Schlomka, J.P.; Roessl, E.; Dorscheid, R.; Dill, S.; Martens, G.; Istel, T.; Baumer, C.; Herrmann, C.; Steadman, R.; Zeitler, G., et al. Experimental feasibility of multi-energy photon-counting K-edge imaging in pre-clinical computed tomography. *Physics in medicine and biology* **2008**, *53*, 4031-4047, doi:10.1088/0031-9155/53/15/002.
15. Ashton, J.R.; Clark, D.P.; Moding, E.J.; Ghaghada, K.; Kirsch, D.G.; West, J.L.; Badea, C.T. Dual-energy micro-CT functional imaging of primary lung cancer in mice using gold and iodine nanoparticle contrast agents: a validation study. *PLoS One* **2014**, *9*, e88129, doi:10.1371/journal.pone.0088129.
16. Stangl, S.; Tei, L.; De Rose, F.; Reder, S.; Martinelli, J.; Sievert, W.; Shevtsov, M.; Ollinger, R.; Rad, R.; Schwaiger, M., et al. Preclinical Evaluation of the Hsp70 Peptide Tracer TPP-PEG24-DFO[(89)Zr] for Tumor-Specific PET/CT Imaging. *Cancer Res* **2018**, *78*, 6268-6281, doi:10.1158/0008-5472.CAN-18-0707.
17. Stangl, S.; Varga, J.; Freysoldt, B.; Trajkovic-Arsic, M.; Siveke, J.T.; Greten, F.R.; Ntziachristos, V.; Multhoff, G. Selective in vivo imaging of syngeneic, spontaneous, and xenograft tumors using a novel tumor cell-specific hsp70 peptide-based probe. *Cancer Res* **2014**, *74*, 6903-6912, doi:10.1158/0008-5472.CAN-14-0413.
18. Cormode, D.P.; Si-Mohamed, S.; Bar-Ness, D.; Sigovan, M.; Naha, P.C.; Balegamire, J.; Lavenne, F.; Coulon, P.; Roessl, E.; Bartels, M., et al. Multicolor spectral photon-counting computed tomography: in

vivo dual contrast imaging with a high count rate scanner. *Scientific reports* **2017**, *7*, 4784, doi:10.1038/s41598-017-04659-9.

19. Si-Mohamed, S.; Cormode, D.P.; Bar-Ness, D.; Sigovan, M.; Naha, P.C.; Langlois, J.B.; Chalabreysse, L.; Coulon, P.; Blevis, I.; Roessl, E., et al. Evaluation of spectral photon counting computed tomography K-edge imaging for determination of gold nanoparticle biodistribution in vivo. *Nanoscale* **2017**, *9*, 18246-18257, doi:10.1039/c7nr01153a.
20. Schubertova, V.; Martinez-Veracoechea, F.J.; Vacha, R. Influence of ligand distribution on uptake efficiency. *Soft Matter* **2015**, *11*, 2726-2730, doi:10.1039/c4sm02815e.
21. Lammers, T.; Kiessling, F.; Hennink, W.E.; Storm, G. Drug targeting to tumors: principles, pitfalls and (pre-) clinical progress. *Journal of controlled release : official journal of the Controlled Release Society* **2012**, *161*, 175-187, doi:10.1016/j.jconrel.2011.09.063.
22. Zhang, X.D.; Wu, H.Y.; Wu, D.; Wang, Y.Y.; Chang, J.H.; Zhai, Z.B.; Meng, A.M.; Liu, P.X.; Zhang, L.A.; Fan, F.Y. Toxicologic effects of gold nanoparticles in vivo by different administration routes. *International journal of nanomedicine* **2010**, *5*, 771-781, doi:10.2147/IJN.S8428.
23. Dorsey, J.F.; Sun, L.; Joh, D.Y.; Witztum, A.; Kao, G.D.; Alonso-Basanta, M.; Avery, S.; Hahn, S.M.; Al Zaki, A.; Tsourkas, A. Gold nanoparticles in radiation research: potential applications for imaging and radiosensitization. *Transl Cancer Res* **2013**, *2*, 280-291, doi:10.3978/j.issn.2218-676X.2013.08.09.
24. Muddineti, O.S.; Ghosh, B.; Biswas, S. Current trends in using polymer coated gold nanoparticles for cancer therapy. *Int J Pharm* **2015**, *484*, 252-267, doi:10.1016/j.ijpharm.2015.02.038.
25. Hainfeld, J.F.; Dilmanian, F.A.; Zhong, Z.; Slatkin, D.N.; Kalef-Ezra, J.A.; Smilowitz, H.M. Gold nanoparticles enhance the radiation therapy of a murine squamous cell carcinoma. *Physics in medicine and biology* **2010**, *55*, 3045-3059, doi:10.1088/0031-9155/55/11/004.
26. Rothammer, A.; Sage, E.K.; Werner, C.; Combs, S.E.; Multhoff, G. Increased heat shock protein 70 (Hsp70) serum levels and low NK cell counts after radiotherapy - potential markers for predicting breast cancer recurrence? *Radiat Oncol* **2019**, *14*, 78, doi:10.1186/s13014-019-1286-0.
27. Pan, C.; Schoppe, O.; Parra-Damas, A.; Cai, R.; Todorov, M.I.; Gondi, G.; von Neubeck, B.; Bogurcu-Seidel, N.; Seidel, S.; Sleiman, K., et al. Deep Learning Reveals Cancer Metastasis and Therapeutic Antibody Targeting in the Entire Body. *Cell* **2019**, *179*, 1661-1676 e1619, doi:10.1016/j.cell.2019.11.013.